WAVELET ANALYSIS OF THE SINGULAR SPECTRAL RECONSTRUCTED TIME SERIES TO STUDY THE IMPRINTS OF SOLAR-ENSO-GEOMAGNETIC ACTIVITY ON INDIAN CLIMATE

[1]S. Sri Lakshmi* and [2]R. K. Tiwari

[1] University Centre for Earth and Space Sciences, University of Hyderabad, Hyderabad 500 046, India

[2] CSIR-National Geophysical Research Institute, Uppal Road, Hyderabad 500 007, India

***Corresponding Author:** srilakshmi.ucess@gmail.com
Tel.: +91-40-23132671 (Office)
Fax: +91-40-23010152

ABSTRACT

To study the imprints of Solar-ENSO-Geomagnetic activity on the Indian Subcontinent, we have applied the Singular spectral analysis (SSA) and wavelet analysis to the tree ring temperature variability record from the Western Himalayas. The other data used in the present study are the Solar Sunspot Number (SSN), Geomagnetic Indices (aa Index) and Southern Oscillation Index (SOI) for the common time span of 1876-2000. Both SSA and wavelet spectral analyses reveal the presence of 5-7 years short term ENSO variations to 11 year solar cycle indicating the possible combined influences of solar-geomagnetic activities and ENSO on the Indian temperature. Another prominent signal corresponding to 33-year periodicity in tree ring record suggests the Sun-temperature variability link probably induced by changes in the basic state of the earth's atmosphere. In order to complement the above findings we performed wavelet analysis of SSA reconstructed time series, which agrees well with our earlier results and also increases the signals to noise ratio thereby showing strong influence of solar-geomagnetic & ENSO throughout the entire time period. The solar flares are considered to be responsible for causing the atmosphere circulation patterns. The net effect of solar-geomagnetic processes on temperature record might suggest counteracting influences on shorter (about 5–6 y) and longer (about 11–12 y) time scales. The present analyses suggest that the influence of solar activities on Indian temperature variability operates in part indirectly through coupling of ENSO on multilateral time scales. The analyses, hence, provide credible evidence for tele-connections of tropical pacific climatic variability and Indian climate ranging from inter-annual-decadal time

scales and also suggest possible role of exogenic triggering in reorganizing the global earth-ocean-atmospheric systems.

Key words: Geomagnetic activity, Western Himalayas, Sunspot Number, SOI index, Singular spectral analysis, Wavelet spectrum, Coherency.

1. Introduction:

Several recent studies of solar/geomagnetic effects on climate have been examined on both global as well as on regional scales (Lean and Rind, 2008; Benestaed and Schmidt, 2009; Meehl, 2009; Kiladis and Diaz 1989; Pant and Rupa Kumar 1997; Gray et al. 1992; Wiles et al. 1998; Friis and Svensmark 1997; Rigozo et al. 2005; Feng et al. 2003; Tiwari and srilakshmi 2009; Chowdary et al. 2006, 2014; Appenzeller et al. 1998; Proctor et al. 2002; Tsonis et al. 2005; Freitas and Mclean 2013). The Sun's long-term magnetic variability caused by the sunspots is considered as one of the primary drivers of climatic changes. The short-term magnetic variability is due to the disturbances in Earth's magnetic fields caused by the solar activities and is indicated by the geomagnetic indices. The Sun's magnetic variability modulates the magnetic and particulate fluxes in the heliosphere. This determines the interplanetary conditions and imposes significant electromagnetic forces and affects upon the planetary atmosphere. All these effects are due to the changing solar-magnetic fields, which are relevant for planetary climates including the climate of the Earth. The Sun-Earth relationship varies on different time scales ranging from days to years bringing a drastic influence on the climatic patterns. The ultimate cause of solar variability, at time scales from decadal to centennial to millennial or even longer scales has its origin in the solar dynamo mechanism. During the solar maxima, huge amounts of solar energy particles are released, thereby causing the geomagnetic disturbances. The 11 years solar cycle acts as an important driving force for variations in the space weather, ultimately giving rise to climatic changes. It is, therefore, imperative to understand the origin of space climate by analyzing the different proxies of solar magnetic variabilities. Another most important phenomena is El Nino-Southern Oscillation (ENSO), which produces droughts, floods and intense rainfall. The strong coupling and interactions between the Tropical Ocean and atmosphere play a major role in the development of global climatic system. The El Nino events generally recur approximately every 3-5 years with large events spaced around 3-7 years apart. The ENSO phenomena have shown huge impact on the Asian monsoon (Cole et. al., 1993), Indian monsoon (Chowdary et al. 2006, 2014) as well as globally (Horel and Wallance 1981; Barnett 1989; Yasunari 1985; Nicholson 1997). In particular, the El Nino, solar, geomagnetic activities are the major affecting forces on the decadal and interdecadal temperature variability on global and regional scales in a direct/indirect way (Gray et al., 2010). Recent studies (Frohlich and Lean 2004; Steinhilber et al. 2009) indicate the possible influence of solar activity on Earth's temperature/climate on multi-decadal time scales. The 11 year solar cyclic variations observed from the several temperature climate records also suggest the impact of solar irradiance variability on terrestrial temperature (Budyko 1969; Friis and Lassen 1991; Friis and Svensmark 1997; Kasatkina et al. 2007). The bi-decadal (22 years) called the Hale cycle, is related to the reversal of the solar magnetic field direction (Lean et al. 1995; Kasatkina et al. 2007). The 33 year cycle (Bruckener cycle) is also caused by the solar origin, but it is a very rare cycle (Kasatkina et al. 2007). The 2–7 years ENSO cyclic pattern and its possible coupling process is the major driving force for the temperature variability (Gray et al. 1992; Wiles et al. 1998; Mokhov et al. 2000; Rigozo et al. 2007, Kothawale et al. 2010). El-Borie et al, 2010 have indicated the possible contributions for both the solar and geomagnetic indices. El-Borie and Al–Thoyaib, 2006 and El-Borie et al., 2007 have indicated in their studies that the global temperature should lag the geomagnetic activity with a maximum correlation when the temperature lags by 6 years. Mendoza et. al., 1991 reported on possible connections between solar activity and El Nino's, while Reid and Gage (1988) and Reid (1991) reported on the similarities between the 11-year running means of monthly sunspot numbers and global sea surface temperature. These findings suggest that there is possibility of strong coupling between temperature-ENSO and solar-geomagnetic signals.

The mean global temperature of the Earth's surface also plays a very important role in bringing climatic changes. Several studies have been carried out to understand the detailed climatic changes of India in the past millennium using various proxy records e.g. ice cores, lake sediments, glacier fluctuations, peat deposits etc. The availability of high-precision and high-resolution palaeo-climatic information for longer time scale from the Indian subcontinent is very less. In recent years, tree-ring data is promising proxy to retrieve high resolution past climatic changes from several geographical regions of India (Bhattacharyya et al. 1988; Bhattacharyya et al. 1992; Hughes, 1992; Bhattacharyya and Yadav, 1996; Borgaonkar et al. 1996; Chaudhary et al. 1999; Yadav et al. 1999; Bhattacharyya and Chaudhary, 2003; Bhattacharyya et al. 2006; Shah et al. 200) It has been noted that tree-ring based climatic reconstructions in India generally do not exceed beyond 400 years records except at some sites in the Northwest Himalaya. Thus, a long record of tree-ring data is needed to extend available climate reconstruction further back to determine climatic variability in sub-decadal, decadal and century scale. However, non availability of older living trees in most of the sites is hindering the preparation of long tree chronology. In previous study (Tiwari and Srilakshmi, 2009) have studied the periodicities and non-stationary modes in the tree ring temperature data from the same region (AD 1200-2000). To gain significant connections among the Solar-geomagnetic-ENSO 'triad' phenomena on tree ring width in detail for the time period from 1876-2000, we have applied here the Singular spectral analysis (SSA) and the wavelet spectral analysis for Sunspot data, geomagnetic data (aa index), Troup Southern Oscillation Index (SOI) and the Western Himalayas tree ring data. Our main objective here is to present a wavelet-based analysis of SSA reconstructed time series to focus on the evidence of the ENSO–solar-geomagnetic connections in comparison to ENSO–geomagnetic and solar–ENSO connections.

2. Source and Nature of Data:

The data analyzed here includes the time series of (1) Smoothed Sunspot number for solar activity (2) Geomagnetic activity data (aa indices) (3) Troup Southern Oscillation Index (SOI) for the study of El Nino-Southern Oscillation called ENSO (4) Western Himalayan temperature variability record. All the data sets have been analyzed for a common period of 125 years spanning over 1876-2000. The monthly sunspot number data has been obtained from the Sunspot Index Data Center http:// astro.oma.be/SIDC/. The Troup SOI data is obtained from the Bureau of Meteorology of Australia, http://www.bom.gov.au/climate/. The data for geomagnetic activity, aa Index, was provided by the National Geophysical Data Center, NGDC, (http://www.ngdc.noaa.gov/stp/GEOMAG/aastar.shtml). The aa index is a measure of disturbances level of Earth's magnetic field based on magnetometer observations at two, nearly antipodal, stations in Australia and England. In recent studies, the tree ring proxy climate indicators have been potentially used for extracting information regarding past seasonal temperature or precipitation/drought based on the measurements of annual ring width. The detailed description of the data has been presented elsewhere (Yadav et. al., 2004). A brief account of the data pertinent to the present analysis, however, is summarized here. The tree ring data being analyzed here is one of the best temperature variability records (1876 to 2000) of the pre-monsoon season in the Western Himalayas. The mean temperature series is obtained from nine weather stations including both from high and low elevation areas in the Western Himalayas. Temperature variability history is based on widely spread pure Himalayan cedar (Cedrus deodara (Roxb.) G. Don) trees and characterizes all the sites with almost no ground vegetation and thereby minimizes individual variation in tree-ring sequences induced by inter tree competition (Yadav et. al., 2004). The mean chorological structure is based on in total 60 radii from 45 trees, statistical feature of which show that the chronology is suitable for dendro-climatic studies back to AD 1226 (Yadav et. al., 2004).

(Figure 1)

3. Methods applied: To analyze the temporal series and to find the climatic structure, we have here applied three methods: Principal component analysis (PCA), Singular Spectral analysis (SSA) and wavelet analysis.

3.1. Principal component analysis (PCA): As a preliminary analysis, we have applied the Principle component analysis (PCA) to the data sets to extract the principle components. PCA technique is applied for the reduction and extraction for dimensionality of the data and to rate the amount of variation present in the original data set. The purpose to apply the PCA is to identify patterns in the given time series. The new components thereby obtained by the PCA analysis are termed as PC1, PC2, PC3 and so on, (for the first, second and third principal components) are independent and decrease the amount of variance from the original data set. PC1 (the first component) captures most of the variance; PC2 captures the second most of the variance and so on. These components are treated as climatic factors or climatic structures.

3.2. Singular spectral analysis: The Singular Spectrum Analysis (SSA) method was developed as the new time series method since 1970s. This method is designed to extract as much information as possible from a short, noisy time series without any prior knowledge about the dynamics underlying the series (Broomhead and King, 1986; Vautard and Ghil, 1989). The method is a form of principal component analysis (PCA) applied to lag-corrections structures of the time series. The basic SSA decomposes an original time series into a new series which consists of trend, periodic or quasi-periodic and white noises according to the singular value decomposition (SVD) and provides the reconstructed components (RCs). The basic steps involved in SSA are: decomposition (involves embedding, singular value decomposition (SVD)) and reconstruction (involves grouping and diagonal averaging). Embedding decomposes the original time series into the trajectory matrix; SVD turns the trajectory matrix into the decomposed trajectory matrices. The reconstruction stage involves grouping to make subgroups of the decomposed trajectory matrices and diagonal averaging to reconstruct the new time series from the subgroups.

Step1: Decomposition:

(a) Embedding: The first step in the basic SSA algorithm is the embedding step where the initial time series change into the trajectory matrix. Let the time series be Y = {y_1, ………, y_N} of length N without any missing values. Here the window length L is chosen such that 2 < L < N/2 to embed the initial time series. We map the time series Y into the L lagged vectors, Yi = {y_i,……,y_{i+L-1}} for i = 1…….K, where K = N - L + 1. The trajectory matrix T_Y (L × K dimensions) is written as:

$$T_Y = \begin{pmatrix} Y_1 \\ Y_2 \\ . \\ . \\ Y_K \end{pmatrix} \qquad \text{……………………………………………(1)}$$

(b) Singular Value Decomposition (SVD): Here we apply SVD to the trajectory matrix T_Y to decompose and obtain T_Y=UDV' called eigentriples; where U_i (K × L dimensions;1 < i < L) is an orthonormal matrix; Di (1 < i < L) is a diagonal matrix of order L; V_i (L × L dimensions;1 < i < L) is a square orthonormal matrix.

The trajectory matrix is thus written as $T_Y = \sum_{i=1}^{d} U_i \sqrt{\lambda_i} V_i^T$; ....(2)

where the i[th] Eigen triple of $T_i = U_i \times \sqrt{\lambda_i} \times V_i^T$, I = 1, 2, 3..., d in which d = max(i: $\sqrt{\lambda_i}$ > 0).

Step 2: Reconstruction:

(c) Grouping: Here the matrix Ti is decomposed into subgroups according to the trend, periodic or quasi-periodic components and white noises. The grouping step of the reconstruction stage corresponds to the splitting of the elementary matrices Ti into several groups and summing the matrices within each group. Let I = {i_1,i_2,...., i_p} be the group of indices i_1, ...i_p. Then the matrix T_I corresponding to the group I is defines as T_I=T_{i1}+ T_{i2}+...T_{ip}. The split of the set of indices J=1, 2, . . . ,d into the disjoint subsets I_1, I_2,....I_m corresponds to the equation ()

T=T_{I1}+T_{I2}+...T_{Im}. ....(3)

The sets I_1,....,I_m are called the eigen triple grouping.

(d) Diagonal averaging: The diagonal averaging transfers each matrix T into a time series, which is an additive component of the intital time series Y. If z_{ij} stands for a element matrix Z, the kth term of the resulting series is obtained by averaging z_{ij} over all i, j such that i+j=k+2. This is called diagonal averaging or the Hankelization of the matrix Z. The Hankel matrix HZ, is the trajectory matrix corresponding to the series obtained by the result of diagonal averaging.

Considering equation (3), let X (L × K) matrix with elements x_{ij}, where 1 ≤ i ≤ L, 1 ≤ j ≤ K. Here diagonal averaging transforms matrix X to a series g_0,...,g_{T-1} using the formula:

$$g_k = \begin{cases} \dfrac{1}{k+1}\sum_{m=1}^{k+1} x^*_{m,k-m+2} & 0 \le k < L^* - 1 \\ \dfrac{1}{L^*}\sum_{m=1}^{L^*} x^*_{m,k-m+2} & L^* - 1 \le k < K^* \\ \dfrac{1}{T-k}\sum_{m=k-k^*+2}^{N-k+1} x^*_{m,k-m+2} & K^* - 1 \le k < T \end{cases} \qquad (4)$$

This diagonal averaging by equation (4) applied to the resultant matrix X_{In}, produces time series Y_n of length T. For such signal characteristics, it is essential to examine the time-frequency pattern as to understand whether a particular frequency is temporally consistent or inconsistent. Hence for non-stationary signals, we need a transform that will be useful to obtain the frequency content of the time series/signal as a function of time.

An alternative method for studying the non-stationarity of the time series is wavelet transform. For non-stationary signals, wavelets decomposition would be the most appropriate method because the analyzing functions (the wavelets function) are localized both in time and frequency.

3.3. Wavelet spectral analysis: During the past decades, wavelet analysis has become a popular method for the analysis of aperiodic and quasi-periodic data (Grinsted et. al., 2004; Jevrejeva et. al., 2003; Torrence and Compo, 1998; Torrence and Webster, 1999). In particular, it has become an important tool for studying localized variations of power within a time series. By decomposing a time series into time-frequency space, the dominant modes of variability and their variation with respect to time can be identified. The wavelet transform has various applications in geophysics, including tropical convection (Weng and Lau 1994), the El Niño–Southern Oscillation (Gu and Philander 1995), etc. We have applied the wavelet analysis to analyze the non-stationary signals which permits the identification of main periodicities of ENSO-sunspot-geomagnetic in the time series. The results give us more insight information about the evolution of these variables in frequency-time mode.

A wavelet transform requires the choice of analyzing function Ψ (called “mother wavelet”) that has the specific property of time-frequency localization. The continuous wavelet transform revolves around decomposing the time series into scaling components for identifying oscillations occurring at fast (time) scale and other at slow scales. Mathematically, the continuous wavelets transform of a time series f(t) can be given as:

$$W_{\psi}(f)(a,b) = \frac{1}{\sqrt{a}} \int_{-\infty}^{\infty} f(t)\psi\left(\frac{t-b}{a}\right) dt \quad \text{...........(5)}$$

Here f(t) represents time series, Ψ is the base wavelets function (here we have chosen the Morlet function), with length that is much shorter than the time series f(t). W stands for wavelet coefficients. The variable ‘a’ is called the scaling parameter that determines the frequency (or scale) so that varying ‘a’ gives rise to wavelet spectrum. The factor ‘b’ is related to the shift of the analysis window in time so that varying b represents the sliding method of the wavelet over f(t).

In several recent analyses, complex Morlet wavelet has been found useful for geophysical time series analysis. The Morlet is mostly used to find out areas where there is high amplitude at certain frequencies. The complex Morlet wavelet can be represented by a periodic sinusoidal function with a Gaussian envelope and is excellent for Morlet wavelet may be defined mathematically, as follows:

$$\psi(t) = \pi^{-1/4} e^{-i\omega_0 t} e^{-t^2/2} \quad \text{..........(6)}$$

where ω_0 is a non-dimensional value. ω_0 is chosen to be 5 to make the highest and lowest values of ψ approximately equal to 0.5, thus making the admissibility condition satisfied. The complex valued Morlet transform enables to extract information about the amplitude and phase of the signal to be analyzed. Wavelet transform preserves the self-similarity scaling property, which is the inherent characteristic feature of deterministic chaos. The continuous wavelet transform has edge artifacts because the wavelet is completely localized in time. The cone of influence (COI) is the area in which the wavelet power caused by a discontinuity at the edge has dropped to e^{-2} of the value to the edge. The statistical significance of the wavelet power can be assessed relative to the null hypotheses that the signal is generated by a stationary process with a given background power spectrum (P_k) of first order autoregressive (AR1) process. (Grinsted et. al., 2004)

$$P_k = \frac{1-\alpha^2}{\left|1-\alpha e^{-2i\pi k}\right|^2} \quad \text{..............(7)}$$

where k is Fourier frequency index.

The cross wavelet transform is applied to two time series to identify the similar patterns which are difficult to assess from a continuous wavelet map. Cross wavelet power reveals areas with high common power. The cross wavelet of two time series x (t) and y (t) is defined as W^{XY} =

$W^x W^{y*}$, where * denotes complex conjugate. The cross wavelet power of two time series with background power spectra P_k^X and P_k^Y is given as

$$D\left(\frac{\left|W_n^X(s)W_n^{Y*}(s)\right|}{\sigma X \sigma Y} < p\right) = \frac{Z_v(p)}{v}\sqrt{P_k^X P_k^Y}, \text{.........(8)}$$

where $Z_v(p)$ is the confidence level associated with the probability p for a pdf defined by the square root of the product of the two χ^2 distributions (Torrence and Compo, 1998). The wavelet power is $\left|W_n^X(s)\right|^2$ and the complex argument of $\left|W_n^X(s)\right|$ can be interpreted as the local phase. The cross wavelet analysis gives the correlation between the two time series as function of period of the signal and its time evolution with a 95% confidence level contour. The statistical significance is estimated using red noise model.

Wavelet coherence is another important measure to assess how coherent the cross wavelet spectrum transform is in time frequency space. The wavelet coherence of two time series is defined as (Torrence and Webster, 1998)

$$R_n^2(s) = \frac{\left|S(s^{-1}W_n^{XY}(s))\right|^2}{S(s^{-1}\left|W_n^X(s)\right|^2).S(s^{-1}\left|W_n^Y(s)\right|^2)} \text{...............(9)}$$

where S is a smoothing operator. The smoothing operator is written as S (W) = S_{scale}(S_{time} ($W_n(s)$)), where S_{scale} denotes smoothing along the wavelet scale axis and S_{time} smoothing in time. Here for the morelet wavelet, the smoothing operator is

$$S_{time}(W)\Big|_s = \left(W_n(s) * c_1^{\frac{-t^2}{2s^2}}\right) \text{.....................(10)}$$

$$S_{time}(W)\Big|_s = \left(W_n(s) * c_2\Pi(0.6s)\right)_n\Big| \text{.............(11)}$$

Where c_1 and c_2 are normalization constants and п is the rectangle function. The factor of 0.6 is empirically determined scale decorrelation length of the Morlet wavelet (Torrence and Compo, 1998). The statistical significance level of the wavelet coherence is estimated using the Monte Carlo methods (Grinsted et. al., 2004).

4. Results and Discussion:

We analyzed the data sets spanning over the period of 1876-2000 using the PCA, SSA and wavelet spectral analyses. Figure 1 shows four time series: (1) Smoothed Sunspot number representing solar activities; (2) Geomagnetic (aa indices); (3) Troup Southern Oscillation Index (SOI) for the study of ENSO and (4) Western Himalayan temperature variability record that are analyzed in the present work. From visual inspection it is apparent from Fig. 1 that both WH and SOI data show irregular and random pattern, while sunspot numbers have quasi- cyclic character. Further WH tree ring record also exhibits distinct temperature variability but nonstationary behavior at different scales. This variability might be suggestive of coupled global ocean-atmospheric dynamics or some other factors, such as deforestation, anthropogenic, high latitudinal influence etc (Yadav et. al., 2004).

(Figure 1)

Hence it is quite difficult to differentiate such a complex climate signals visually and difficult to infer any clear oscillation without the help of powerful mathematical methods. For identification of any oscillatory components and understanding the climatic variations on regional and global scale, we have applied the PCA, SSA and wavelet analysis. Figure 2 shows the principal components (PCs) for the first four eigen triples (PC1, PC2, PC3, PC4) for the given data sets. Figure 3 shows the power spectra of the principal components (PCs) for the four data sets shown in figure 2. From the figure 3, it is observed that the power spectra of PC1-4 for the sunspot data exhibits high power at 124, 11, 4-2.8 years. The presence of high solar signal at 124 years indicates the quasi-stable oscillatory components in the data. The power spectra of geomagnetic data also shows the presence of strong signals at 124, 10-11, 4-2 years suggesting a strong link of solar-geomagnetic activity. The power spectra of WH temperature data shows strong high power at ~62 years, 32-35 years, 11 years, 5 years and 2-3 years suggesting a strong influence of solar-geomagnetic-ENSO effects on the Indian climate system. Dominant amplitude is found at 32-35 years corresponding to AMO cycles. These results can be better confirmed by applying the mathematical tools of SSA and wavelet analysis.

(Figure 2 & 3)

To explore the stationary characteristics of these peaks obtained by the PCA, we have applied the Morlet based wavelet transform approach (Holschneider, 1995; Foufoula-Georgiou and Kumar, 1995; Torrence and Compo, 1998; Grinsted et. al., 2004). The wavelet spectrum identifies the main periodicities in the time series and helps to analyze the periodicties with respect to time. Figure 4 shows the wavelet spectrum for the a) Smoothed Sunspot number for solar activity (SSN) (b) Western Himalayan (WH) temperature variability record (c) Geomagnetic activity and (c) Troup Southern Oscillation Index (SOI). From the wavelet spectrum of sunspot time series (Figure 4a), the signal near 11-year is the strongest feature and is persistent during the entire series indicating the non-stationary behavior of the sunspot time series. The wavelet spectrum of SOI (figure 4c) shows strong amplitudes but nonstationary in the interval of 2- 8 years. The wavelet power spectrum of the western Himalayan temperature variability (Figure 4b) reveals significant power concentration at inter-annual time scales of 3-5 years and at 11 years solarcycle. A dominant amplitude modes is also seen in the low frequency range at around 35-40 years (at periods 1930-1980) corresponding to AMO cycles. Our result agrees well with the results of other climate reconstructions (Mann et. al., 1995) from tree rings and other proxies. The observed variability in AMO periodicity has also been reported in other tree ring record (Gray et. al., 2004). The statistical significance of the wavelet power spectrum is tested by a Monte Carlo method (Torrence and Compo, 1998). The WH spectra depicting statistically significant powers at around 5 years, 11 years and 33 years above the 95% significance level, suggests a clear picture of the imprint of sunspot-geomagnetic and ENSO on the tree ring data. The wavelet power spectrum of the geomagnetic record (Fig. 4d) indicates significant power on shorter scales around 2, 4-8, 11 years period.

(Figure 4)

In order to have better visualization of similar periods in two time series and for the interpretation of the results, cross wavelet spectrum has been applied. Figure 5 shows the cross wavelet spectrum of the a) SSN-WH temperature data b) WH data-SOI and c) SSN-SOI data. The contours (dark black lines) are the enclosing regions where wavelet cross power is significantly higher, at 95% confidence levels. The wavelet cross-spectra of WH-SSN (Fig.5a) show statistically significant high power over a period of 1895-1985 in 8-16 years band. It is seen that the WH-SOI cross-spectra (Fig. 5b), the high power is observed at 2–4 year band and 8–16 years as well. The SSN-SOI spectra (Fig. 5c) shows a strong correlation at 11 years solar cycle, which is stronger during 1910-1950 and 1960-2000 (Rigozo et. al., 2002, Rigozo et. al., 2003) suggesting the strongest El Nino and La Nina events indicating solar modulation on ENSO. These results show a good correspondence in response of growth of the tree ring time series during the intense solar activity. Hence the results strongly support the possible origin of these periodicities from Solar and ENSO events. The interesting conclusion from Fig. 5 is that WH–sunspot connections are strong at 11 years, ENSO–sunspot also exhibit strong power around 11 years; the WH–ENSO connections are spread over three bands, the 2–4 y; 4–8 and 8–16 y, covering the solar cycle and its harmonics; the WH-geomagnetic exhibits strong connections around 2-4, 4-6, 11 years and 35-40 years indicating the influence of solar-geomagnetic activity on Indian temperature.

(Figure 5)

The Singular spectral analysis (SSA) is performed for all the four data sets with window length of 40. The SSA spectra with 40 singular values and its corresponding reconstructed series (varying from RC1-15 in some cases) are plotted are shown in Figure 6 &7. The important insights from SSA spectra are the identification of gaps in the eigen value spectra. As a rule, the pure noise series produces a slowing decreasing sequence of singular values. The explicit plateau in the spectra represents the ordinal numbers of paired eigen triples. The eigen triples 2-3 for the sunspot data corresponds to 11 years period; eigen triples for 1-2,3-5,6-10,11-14 for the WH temperature data are related to harmonic with specific periods (periods 33-35, 11, 5, 2); eigen triples for 2-5,6-9,10-13 for the geomagnetic data are related to periods 11, 5,2 years. The eigen triples for the SOI data represents to ~ 5-7, 2 years periods. In order to assess periodicities, the periodogram and the wavelet power spectra are plotted using the SSA reconstructed data (SSA-RC) (Figure 8). From the figure 8, the periodogram of SSA-RC of SSN and Geomagnetic data shows strong power at ~120, 10-11 years; the SOI data shows strong peaks at 6-9, 3, years & WH data shows strong power at ~32, ~10-11, 3-5 years. The wavelet spectra for all the SSA-RC data confirms the results excepts for periods at ~120 years as the scaling period for the wavelet spectra is 64 years period. The coherency plot of the SSA-RC data sets (Figure 9) indicates a significant power at 33 years, 11 years, 2-7 years in the WH temperature record suggesting the possible influences of Sunspot-geomagnetic activity and ENSO through tele-connection and hence significant role of these remote internal oscillations of the atmosphere-ocean system on the Indian climate system. Researchers have attributed these phenomena to internal ocean dynamics and involve ocean atmospheric coupling as well as variability in the strength of thermohaline circulations (Knight et. al., 2005; Delworth and Mann, 2000).

(Figures 6, 7, 8 & 9)

In general our result agrees well with earlier findings in sense that statistically significant global cycles of coupled effects of Sunspot/geomagnetic and ENSO are present in the land based temperature variability record. However, there are certain striking features in the spectra that need to be emphasized regarding the western Himalayas temperature variability: i) Inter-annual cycles in period range of 3-8 years corresponding to ENSO in the wavelet spectra exhibit intermittent oscillatory characteristics throughout the large portion of the record (Fig 4); ii) The 11 years solar cycle in the cross wavelet spectrum of SSN and SOI (Figure 5) indicate the solar modulation in the ENSO phenomena. iii) The high amplitude at 11 years in the time intervals 1900-1995 with a strong intensity from 1900-1995 shows a good correspondence with the high temperature variability for the interval of high solar-geomagnetic activity. The Multi-decadal (30-40 years) periodicity identified here in Western Himalayan tree ring temperature record matches with North Atlantic sea surface temperature variability implying that the temperature variability in the western Himalayan is not a regional phenomenon, but a globally tele-connected climate phenomena associated with the global ocean-atmospheric dynamics system (Tiwari & srilakshmi, 2009; Delworth et. al., 1993; Stocker, 1994). The coupled ocean-atmosphere system appears to transport energy from the hot equatorial regions towards Himalayan territory in a cyclic manner. These results may provide constraints for modeling of climatic variability over the Indian region and ENSO phenomena associated with the redistribution of temperature variability. The solar-geomagnetic effects play a major role in abnormal heating of the land surface thereby indirectly affects the atmospheric temperature gradient between the land-ocean coupled systems. In the present work, the connections between solar/geomagnetic activity and ENSO on the WH time series are found to be statistically significant, especially when they are studied over contrasting epochs of respectively high and low solar activity. The correlation plots for the SSA-RC data sets of WH-sunspot, WH-aa index, WH-SOI and Sunspot-aa index are plotted in figure 10. It is noticed that there is a correlation plots for the Geomagnetic-sunspot activity has a maximum correlation value at 1 year lag suggesting the strong influence of sunspot & geomagnetic forcing on one another. The cross-correlation plot for the WH data and the SOI represents a maximum value at zero lag. The correlations plot for WH-sunspot & WH-geomagnetic index exhibits almost the identical results suggesting the possible impact of solar activities on the Indian temperature variability.

(Figures 10)

The net effect of solar activity on temperature record therefore appears to be the result of cooperating or counteracting influences of earth's magnetic activity on the shorter and longer periods, depending on the indices used; scale-interactions, therefore, appear to be important. Nevertheless, the link between Indian climate and solar/geomagnetic activity emerges as having the strong evidence; next is the ENSO–solar activity connection.

5. Conclusions:

In the present paper, we have studied & identified the periodic patterns from the published Indian temperature variability records using the modern spectral methods. This study of Singular spectral analysis (SSA)-Wavelet spectral methods on the data sets and the application of wavelet analysis for the SSA reconstructed time series highlights the removal of noise in the data and identifies the existence of a high-amplitude, recurrent, multi-decadal scale patterns that are present in Indian temperature records. The Wavelet spectral analysis of SSA reconstructed data identifies significant peaks around 33 years, 11 years, 2-7 years (95%

confidence) in the Western Himalayan (WH) temperature record. The presence of 33-year cycle periodicity suggests the Sun-temperature variability probably involving the induced changes in the basic state of the atmosphere. The 30-40 yrs periodicity in Western Himalayan tree ring temperature record matches with the global signal of the coupled ocean-atmospheric oscillation (Delworth et. al., 1993; Stocker, 1994) implying that the temperature variability in Himalayan is not a regional phenomenon, but seems to be tele-connected phenomena with the global ocean-atmospheric climate system. The coherency plots of the SSA reconstructed WH-Sunspot; WH-geomagnetic and WH-SOI data sets show strong spectral signatures in the whole record confirming the possible influences of Sunspot-geomagnetic activities and ENSO through teleconnection and hence the significant role of these remote internal oscillations of the atmosphere-ocean system on the Indian temperatures. We conclude that the signature of solar-geomagnetic activity affects the surface air temperatures of Indian subcontinent. However, long data sets from the different sites on the Indian continent are necessary to identify the influences of the 120 years solar-geomagnetic cycles.

Acknowledgements

The authors are extremely thankful to the anonymous reviewers for their professional comments, meticulous reading of the manuscript and valuable suggestions to improve the manuscript. The authors thank Dr. R. R. Yadav for providing "his" data. We are thankful to Dr. Grinsted and his colleagues for providing the wavelet software package. We are very grateful to the Head, UCESS, University of Hyderabad for his support and kind permission to publish this paper.

References

Appenzeller, C., Stocker, T. F., and Anklin, M. (1998). North Atlantic Oscillation Dynamics Record in Greenland Ice Cores. Science, 282(5388), 446–449.

Barnett, T.P., et al. (1989). The effect of Eurasian snow cover on regional and global climate variations. J. Atmos. Sci., 48, 661–685.

Benestaed, R.E., and Schmidt, G.A., (2009), Solar trends and global warming, Journal of Geophysical research, P 114.

Bhatacharyya A, LaMarche VC, and Telewski FW, (1988) Dendrochronological reconnaissance of the conifers of Northwest India, Tree-Ring Bull., 48: 21-30.

Bhattacharyya A, and Chaudhary V, (2003) Late-summer temperature reconstruction of the Eastern Himalayan Region based on tree-ring data of Abies densa, Arct. Antarct. Alp.Res., 35(2): 196-202.

Bhattacharyya A, and Yadav RR, (1996) Dendrochronological reconnaissance of Pinus wallichiana to study glacial behaviour in the western Himalaya. Current Science, 70 (8): 739-744.

Bhattacharyya A, Shah, Santosh K, and Chaudhary V, (2006) Would tree-ring data of Betula utilis be potential for the analysis of Himalayan Glacial fluctuations?, Current Science, 91(6): 754-761.

Bhattacharyya A, Yadav RR, Borgaonkar HP, & Pant GB, (1992) Growth ring analysis of Indian tropical trees: Dendroclimatic potential, Current Science, 62: 736-741.

Bhattacharyya, A. and Yadav, R.R., (1992) Tree growth and recent climatic changes in the western Himalaya, GeophytoJogy, 22, 255-260.

Bigg GR, (1996) The oceans and Climate, Cambridge University Press, Cambridge, 1-266.

Borgaonkar HP, Pant GB, & Rupa Kumar k, (1996) Ring width variations in Cedrus deodara and its climatic response over the Western Himalaya. Intern. J. Climatol. 16: 1409-1422.

Broomhead, D.S., and King, G.P., (1986). Extracting qualitative dynamics from experimental data, Physica D 20, 217–236.

Budyko, M. I. (1969). The effect of solar radiation variations on the climate of the Earth. Tellus, 21, 611–619

Cane MA, (1992) Tropical Pacific ENSO models: ENSO as a mode of the coupled system. In: Climate System Modelling, Ed: K.E. Trenberth, Cambridge University Press, Cambridge, 583-614.

Chaudhary V, Bhattacharyya A, and Yadav RR, (1999) Tree-ring studies in the Eastern Himalayan region: Prospects and problems, IAWA, .20(3): 317-324.

Chowdary, J. S., John, N., and Gnanseelan, C. (2014). Interannual variability of surface air-temperature over India: impact of ENSO and Indian Ocean Sea surface temperature. Int. J. Climatol., 34, 416–429.

Chowdary, J.S., Gnanseelan, C., Vaid, B.H., and Salvekar, P.S. (2006). Changing trends in the tropical Indian Ocean SST during La Nina years. Geophys. Res. Lett., 33, L18610. doi:10.1029/ 2006GL026707.

Cole JE, Fairbanks RG, and Shen GT, (1993) Recent variability in the Southern Oscillation: Isotopic results from a Tarawa Atoll coral. Science, 260: 1790-1793.

De Freitas, C., and Mclean, J. (2013). Update of the Chronology of Natural Signals in the Near-Surface Mean Global Temperature Record and the Southern Oscillation Index. International Journal of Geosciences, 4 (1), 234–239.

Delworth T, and Mann M, (2000) Observed and Stimulated multideacadl variability in the Northern Hemisphere, 16: 661-676.

Delworth T, Manabe S & Stouffer RJ (1993) Interdecadal variations of the thermohaline circulation in a coupled ocean-atmosphere model. J. Climate 6: 1991-2011.

El–Borie, M.A., Shafik, E., Abdel–Halim, A.A., El–Monier, S., (2010), Spectral analysis of solar variability and their possible role on the global warming (1880-2008), Journal of Enviromental Protection, 1, pp 111-120.

El–Borie, M.A., Al. Thoyaib, S.S, Al–Sayed, N., (2007), The 2nd Inter. CPMS, 302.

El-Borie, M.A., and Al-Thoyaib, S.S., (2006), Can we use the aa geomagnetic activity index to predict partially the variability in global mean temperature, Journal of Physical Sci.,1(2), pp 67–74.

Feng, S.H., Kaufman, D., Yoneji, S., Nelson, D., Shemesh, A., Huang, Y., Tian, J., Bond, G., Benjamin, C., and Brown, T. (2003). Cyclic Variation and Solar Forcing of Holocene Climate in the Alaskan Subarctic. Science, 301, 1890–1893.

Foufoula-Georgiou E, and Kumar P, (Eds.), (1995) Wavelets in Geophysics, Academic San Diego, Calif., 373pp.

Friis, C.E., and Lassen, K. (1991). Length of the Solar Cycle: An Indicator of Solar Activity Closely Associated with Climate. Science, 254 (5032), 698–700.

Friis, C.E., and Svensmark, H. (1997). What do we really know about the sun- climate connection?, Adv. Space Res., 20, 415, 913–9211.

Frohlich, C., and Lean, J. (2004). Solar radiative output and its Variability: Evidence and Mechanisms. The Astron Astropys Rev., 12, 273–320.

Gray L.J.,Beer, J., Geller, M., Haigh,J.D., Lockwood, M., Matthes, K., Cubasch, U., Fleitmann,D., Harrison,G., Hood,L., Luterbacher,J., Meehl,G.A., Shindell, D.,vanGeel B., and White, W., (2010). Solar influences on climate, Reviews of Geophysics, 48, RG 4001, doi: 10.1029/2009RG000282.

Gray ST, Graumlich LJ, Betancourt JL, and Pederson GT, (2004) A tree-ring based reconstruction of the Atlantic Multidecadal Oscillation since 1567 A.D, Geophys. Res. Lett. , 31: L12205, doi:10.1029/2004GL019932.

Gray, W. M., Sheaffer, J. D., and Knaff, J. A. (1992). Hypothesized mechanism for stratospheric QBO influence on ENSO variability. Geophy. Res. Let., 19, 107–110.

Grinsted A, Moore JC, Jevrejeva S (2004) Application of the cross wavelet transform and wavelet coherence to geophysical time series, Nonlin. Processes Geophys., 11: 561–566, doi:10.5194/npg-11-561-2004

Gu, D., and Philander, S.G.H., (1995). Secular changes of annual and inter-annual variability in the tropics during the past century, J. Clim. 8, 64–876.

Holschneider M (1995) Wavelets: An Analysis Tool, Oxford University Press, New York, 455.

Horel, J.D., and Wallance, J.M.(1981). Planetary-scale atmospheric Phenomena associated with the Southern Oscillation, Monthly weather review, 109, 813-829.

Hughes MK (1992) Dendroclimatic evidence from the Western Himalaya. In: R.S. Bradlay & D.Jones(eds.),ClimatesinceAD 1500:4 15-431.Routledge.London.

Jevrejeva S, Moore JC, Grinsted A (2003) Influence of the Arctic Oscillation and El Niño-Southern Oscillation (ENSO) on ice conditions in the Baltic Sea: The wavelet approach, J. Geophys. Res., 108(D21), 4677, doi:10.1029/2003JD003417.

Ji JF, Shen J, Balsam W, Chen J, Liu L & Liu XQ, (2005) Asian monsoon oscillations in the northeastern Qinghai-Tibet Plateau since the late glacial as interpreted from visible reflectance of Qinghai Lake sediments, Earth and Planetary Science letters 233: 61-70.

Kasatkina, E.A., Shumilov, O.I., and Krapiec, M.(2007). On periodicities in long term climatic variations near 68_N, 30_E. Adv. Geosci, 13, 25–29.

Kiladis, G.N., and Diaz, F.H. (1989). Global Climatic Anomalies Associated with Extremes in the Southern Oscillation. J. Climate, 2, 1069–1090.

Knight JR, Allan RJ, Folland CK, Vellinga M, and Mann ME, (2005) A signature of persistent natural thermohaline circulation cycles in observed climate'. Geophys. Res. Lett., 32, L20708, doi:10.1029/2005GL024233.

Kothwale, D.R., Munot, A.A., and Krishna Kumar, K. (2010). Surface air temperature variability over India during 1901-2007 and its association with ENSO. Climate Research, 42, 89–104, doi:10.3354/cr00857

Labitzke K and Van Loon H, (1989) Association between the 11-Year Cycle, the QBO and the Atmosphere, Journal of Climate, 2.

Labitzke K and Van Loon H, (1992) Association between the 11-Year solar cycle and the Atmosphere. Part V: Summer, J. Climate, 5: 240-251.

Labitzke K and Van Loon H, (1993) Some recent studies of probable connections between solar and atmospheric variability, Ann. Geophysicae, 11.

Lean and Rind, 2008; Lean, J.L. and Rind, D.H., (2008), How natural and anthropogenic influences alter global and regional surface temperatures: 1889 to 2006, Journal of Geophysical Research, Letter, p 35.

Lean, J., Beer, J., and Bradley, R. (1995). Reconstruction of solar irradiance since 1610: Implications for climate change. Geophy. Res.Lett., 22, 3195-3198.

Mann ME, Park J, and Bradley RS, (1995) Global interdecdal and century-scale climate oscillations during the past 5 centuries, Nature, 378: 266–27.

Meehl, G.A., Arblaster, J.M., Matthes, K., Sassi, F., and Van Loon, H. (2009). Amplifying the Pacific climate system response to a small 11-year solar cycle forcing. Science, 325, 1114–1118.

Mendoza B, Perez-Enriquez R, and Alvarez-Madrigal M, (1991) Analysis of solar activity conditions during periods of El Nino events, Ann. Geophysicae, 9: 50-54.

Mokhov, I. I., Eliseev, A.V., Handorf, D., Petukhov, V.K., Dethloff, K., Weishiemer, A., and Khvorostyanov, D. V. (2000). North Atlantic Oscillation: Diagnosis and simulation of decadal variability and its long period evolution. Atmospheric and Ocean physics, 36, 555–565.

Nicolson, S. E. (1997). An analysis of the Enso signal in the tropical Atlantic and western Indian oceans. Int. J. Climatol., 17, 345–375.

Pant, G.B., and Rupa Kumar, K. (1997). Climates of South Asia. John Wiley and Sons, Chichester, 320 pp.

Philander SG, (1990) El Nino, La Nina and the Southern Oscillation. Academic Press, London, 1-293.

Proctor, C.J., Baker, A., and Barnes, W. L. (2002). A three thousand year record of North Atlantic Climate. Clim.Dyn, 19, 449–454.

Reid GC and Gage KS, (1988) The climatic impact of secular variations in solar irradiance, in Secular Solar and geomagnetic Variations in the Last 10000 years', Eds. F.R. and A.W. Wplfendale, NATO AS Series, Kluwer, Dordrecht, 225-243.

Reid GC, (1991) Solar irradiance variations and global Ocean Temperature, Journal of Geomagn. Geoelectr., 43: 795-801.

Rigozo NR, Noredmann DJR, Echer E, Zanandrea A, Gonzalez WD, (2002) Solar variability effects studied by tree-ring data wavelet analysis,Adv. Space Res., 29(12): 1985-1988.

Rigozo NR, Vieira Lea, Echer E, Nordemann DJR, (2003) Wavelet analysis of Solar-ENSO imprints in tree-ring data from Southern Brazil in the last century, Climatic change, 60: 329-340.

Rigozo, N. R., Nordeman, D. J. R., Echer, E., Vieira, L. E. A., Echer M. P. S. and Presets, A.(2005). Tree-ring width wavelet and spectral analysis of solar variability and climatic effects on a Chilean cypress during the last two and a half millennia. Climate of the Past Discussions, 1, 121–135.

Rigozo, N. R., Nordeman, D.J.R., Silva, H.E., Echer, M.P.S. and Echer, E. (2007). Solar and climate signal records in tree ring width from Chile (AD1587–1994). Planetary and Space Science, 55, 158–164.

Shah Santosh K, Bhattacharyya A, and Chaudhary V, (2007) Reconstruction of June-September Precipitation based on tree-ring data of Teak (Tectona grandis L.) from Hoshangabad, Madhya Pradesh, India. Dendrochronologia, 25: 57-64.

Steinhilber, F., Beer, J. and Frohlich, C. (2009). Total solar irradiance during the Holocene. Geophys. Res. Lett., 36, L19704.

Stocker TF (1994). The variable ocean. Nature 367: 221-222.

Tiwari RK, and Srilakshmi S, (2009). Periodicities and non-stationary modes in tree ring temperature variability record of the Western Himlayas by multitaper and wavelet spectral analyses, Current Science, 97, 5: 705-709.

Torrence C, Compo GP, (1998). A practical guide to wavelet analysis, Bull. Am. Meteorol. Soc., 79: 61–78

Torrence C, Webster P, (1999). Interdecadal changes in the ESNO-Monsoon System, J.Clim., 12: 2679–2690.

Trenberth K, and Hoar TJ, (1997). El Nino and climate change. Geophys. Res. Lett., 24: 3057–3060.

Tsonis, A. A., Elsner, J. B., Hunt, A. G., and Jagger, T. H. (2005). Unfolding the relation between global temperature and ENSO. Geophy.Res.Lett.,32, L09701.

Vautard, R., and Ghil, M. (1989). Singular spectrum analysis in nonlinear dynamics, with applications to paleoclimatic time series. Phys. D, 35, 395–424.

Weng, H., and K.-M. Lau, 1994: Wavelets, period doubling, and time-frequency localization with application to organizationmof convection over the tropical western Pacific. J. Atmos. Sci., 51, 2523–2541.

Wiles, G. C., D'Arrigo, R. D., and Jacoby, G. C. (1998). Gulf of Alaska atmosphere-ocean variability over recent centuries inferred from coastal tree-ring records, Climatic Change, 38,

Yadav RR, Park WK, and Bhattacharyya A, (1999) Spring-temperature variations in western Himalaya, India, as reconstructed from tree-rings: AD 1390-1987, The Holocene, 9(1): 85-90.

Yadav RR, Park WK, Singh J & Dubey B, (2004) Do the western Himalayas defy global warming?', Geophysical Research Letters 31: L17201, doi: 10.1029/2004GL020201.

Yasunari, T. (1985). Zonally propagating modes of the global east–west circulation associated with the Southern Oscillation. J. Meteorol. Soc. J., 63, 1013–1029.

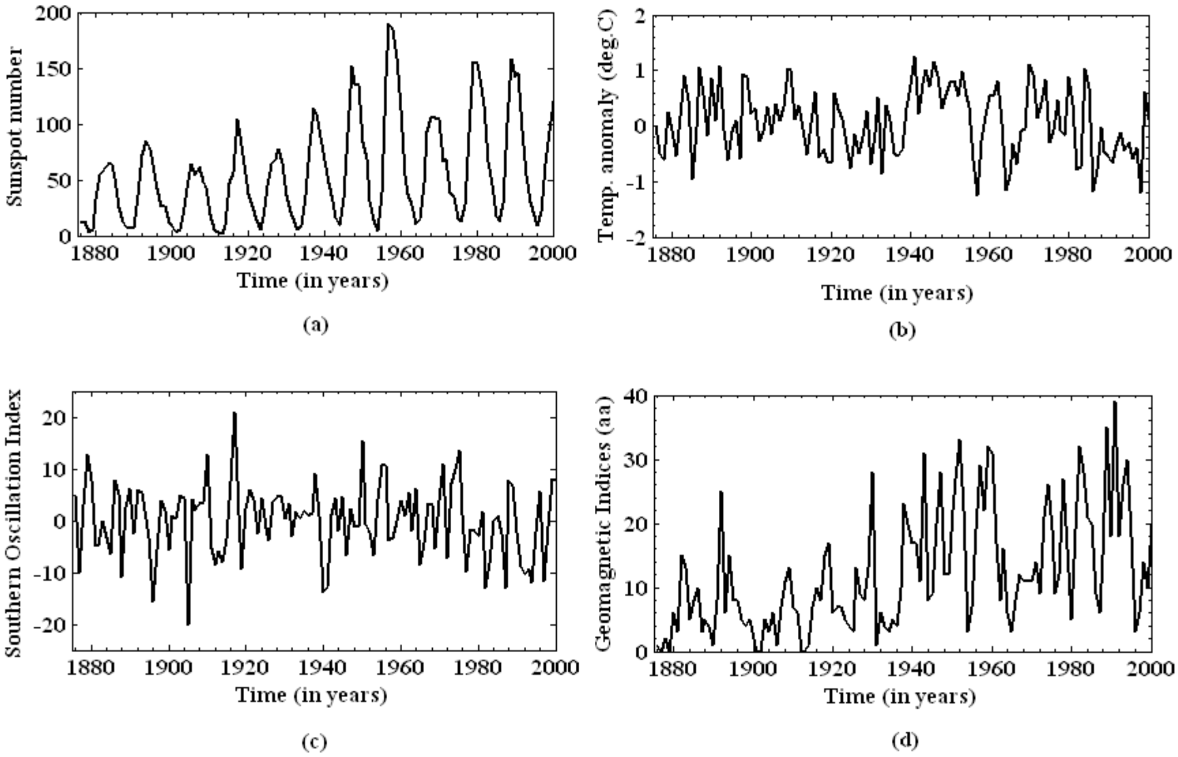

Figure 1. Time series data of (a) Sunspot Index (b) the mean pre-monsoon temperature anomalies of the Western Himalayas (c) Southern Oscillation Index (SOI) and (d) Geomagnetic Indices (aa indices) for common period 1876-2000.

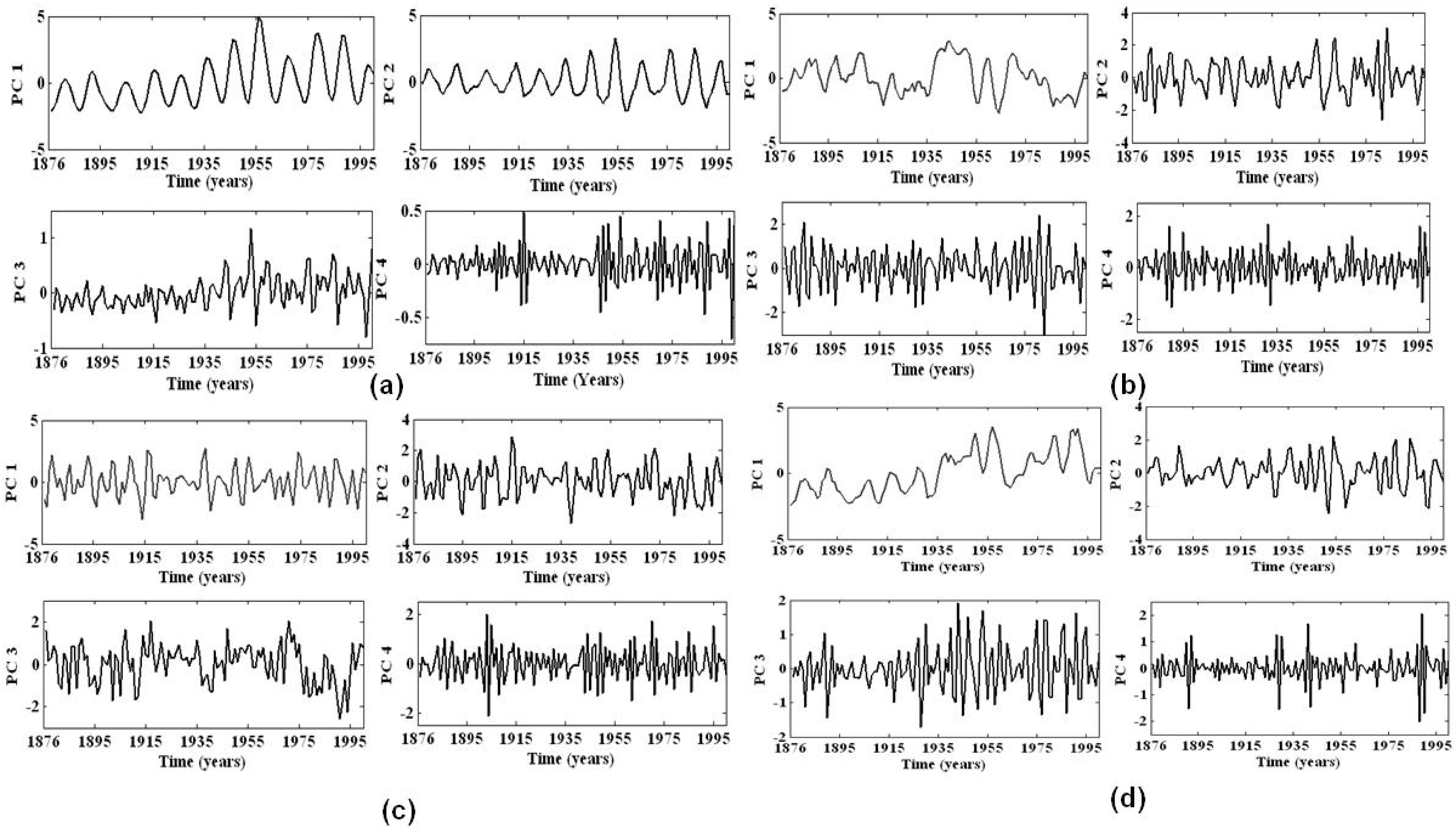

Figure 2. First four principal components (PCs:1-4) for time series (a) Sunspot numbers (b) the mean pre-monsoon temperature anomalies of the Western Himalayas (c) SOI index and (d) Geomagnetic Indices (aa indices) for the period 1876-2000.

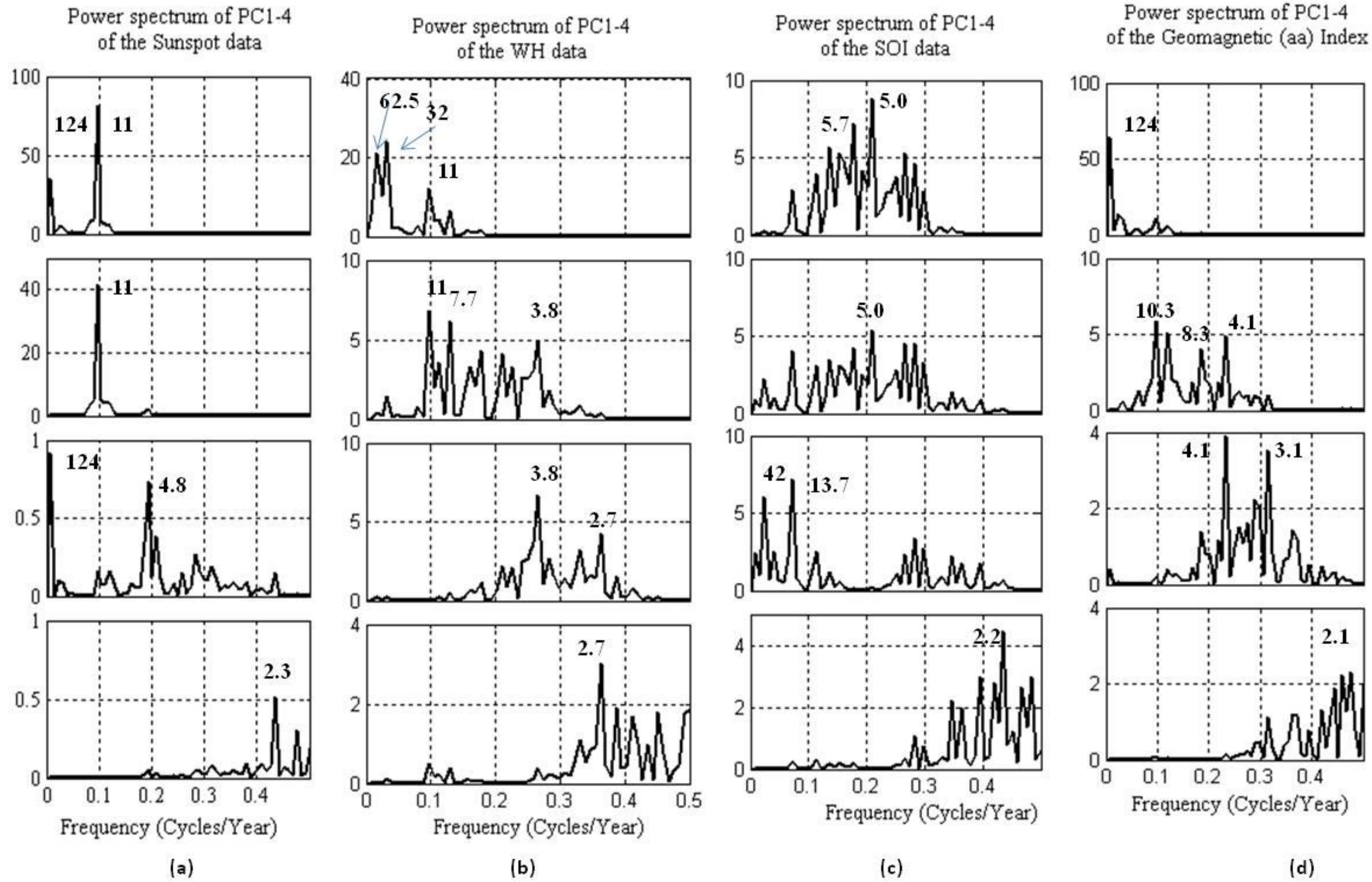

Figure 3. Power spectra of the first four principal component (PCs) (PC1-4 shown in Fig. 2) for all the data sets with their significant periodicities at 124, 11, 4 and 2.8 years are indicated in bold letters.

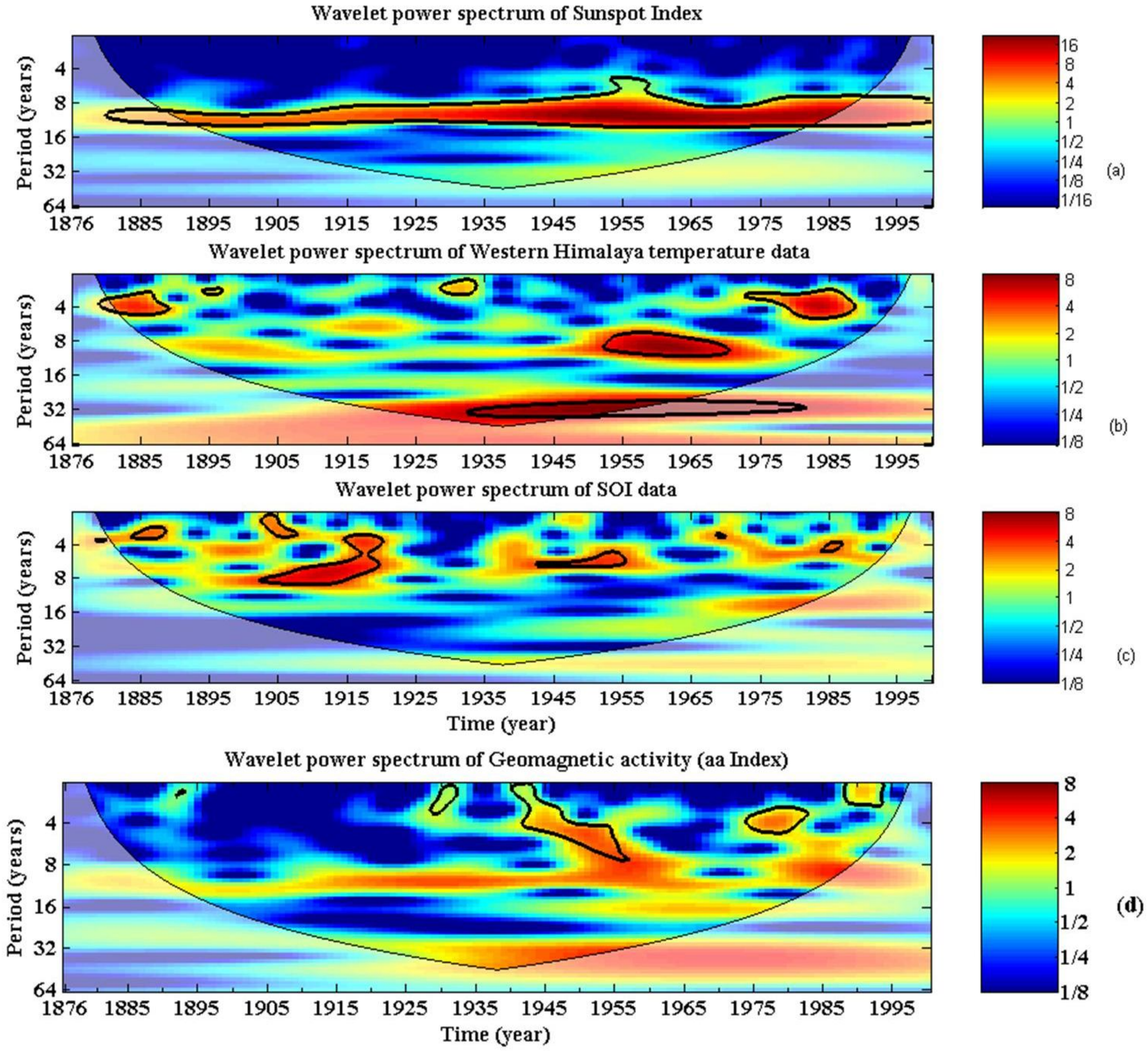

Figure 4. Wavelet power spectrum of (a) Sunspot Number (b) Western Himalaya temperature data (c) Southern Oscillation Index (SOI) and (d) Geomagnetic activity (aa Indices) with cone of influence (lighter shade smooth curve) and black lines indicate significant power on 95% level compared to red noise based on first order auto-regressive (AR(1)) coefficient. The legend on right indicates the cross-wavelet power.

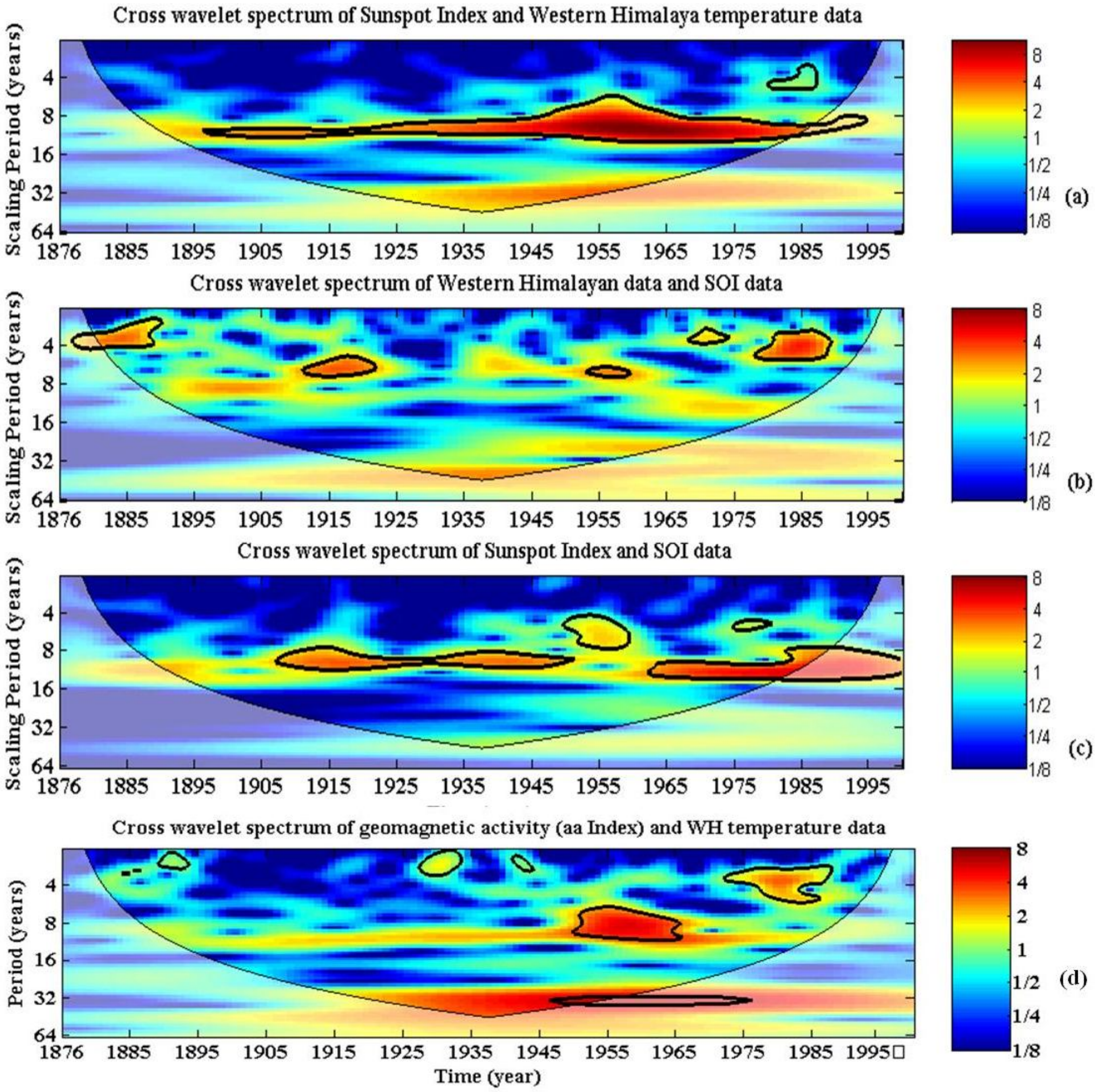

Figure 5. Cross Wavelet spectrum between (a) Sunspot number-Western Himalayan data (b) Western Himalayan-Southern Oscillation Index (c) Sunspot number- Southern Oscillation Index and (d) Geomagnetic: aa indices-Western Himalayan data with cone of influence (lighter shade smooth curve) and black lines indicate significant power on 95% level compared to red noise based on AR(1) coefficient. The legend on right indicates the cross-wavelet power.

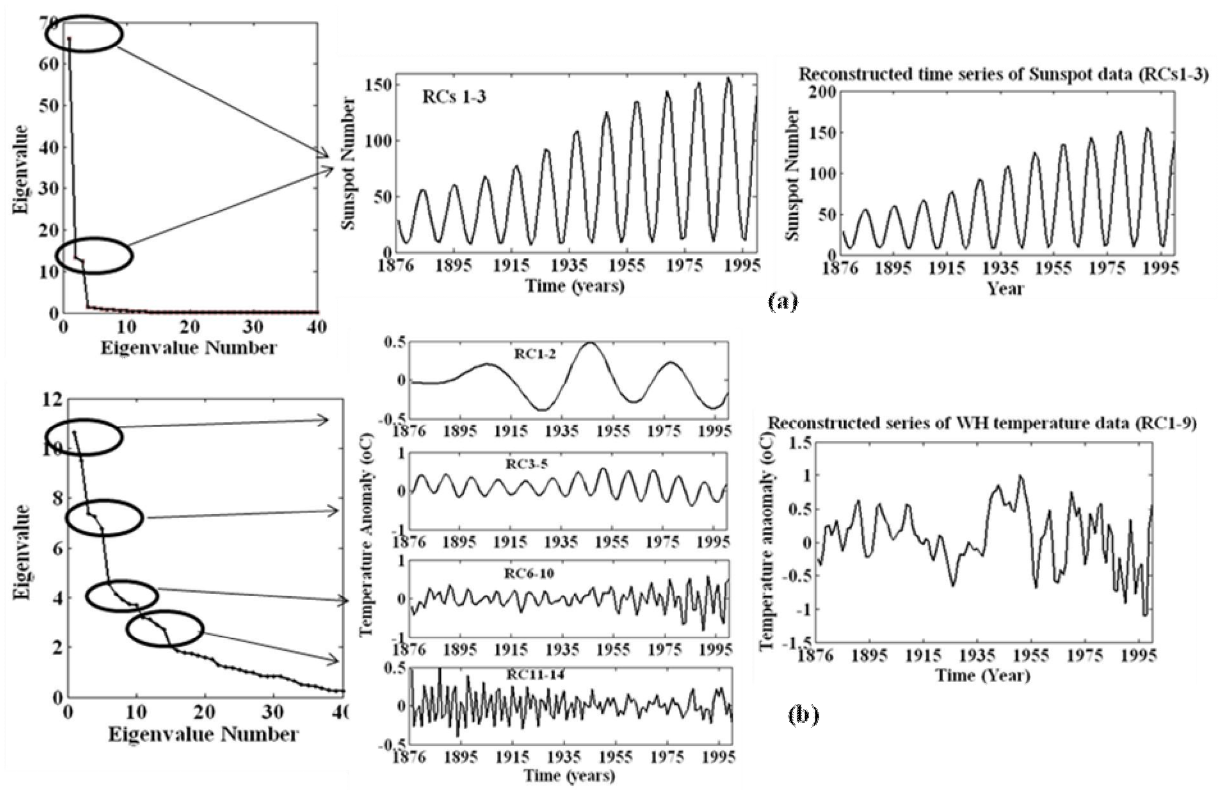

Figure 6. Singular spectra with its SSA decomposed components & its reconstructed time series for (a) Sunspot Number and (b) Western Himalaya temperature data.

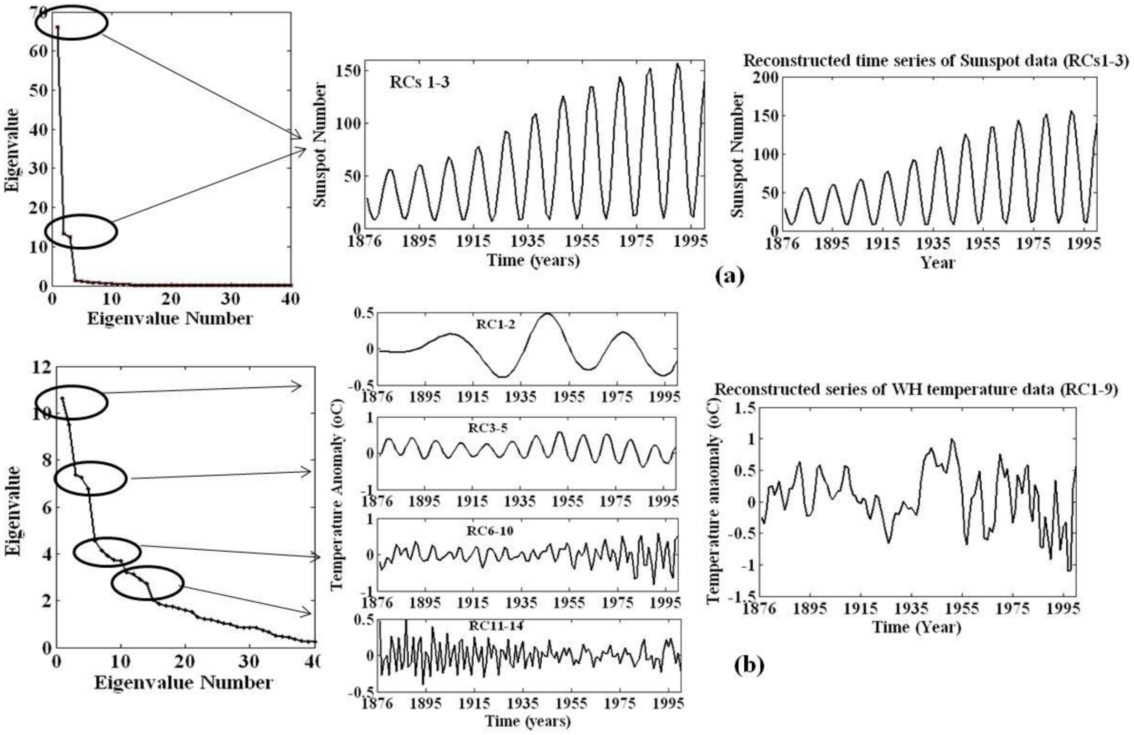

Figure 7. Singular spectra with its SSA decomposed components & its reconstructed time series for (c) SOI and (d) Geomagnetic activity (aa Indices).

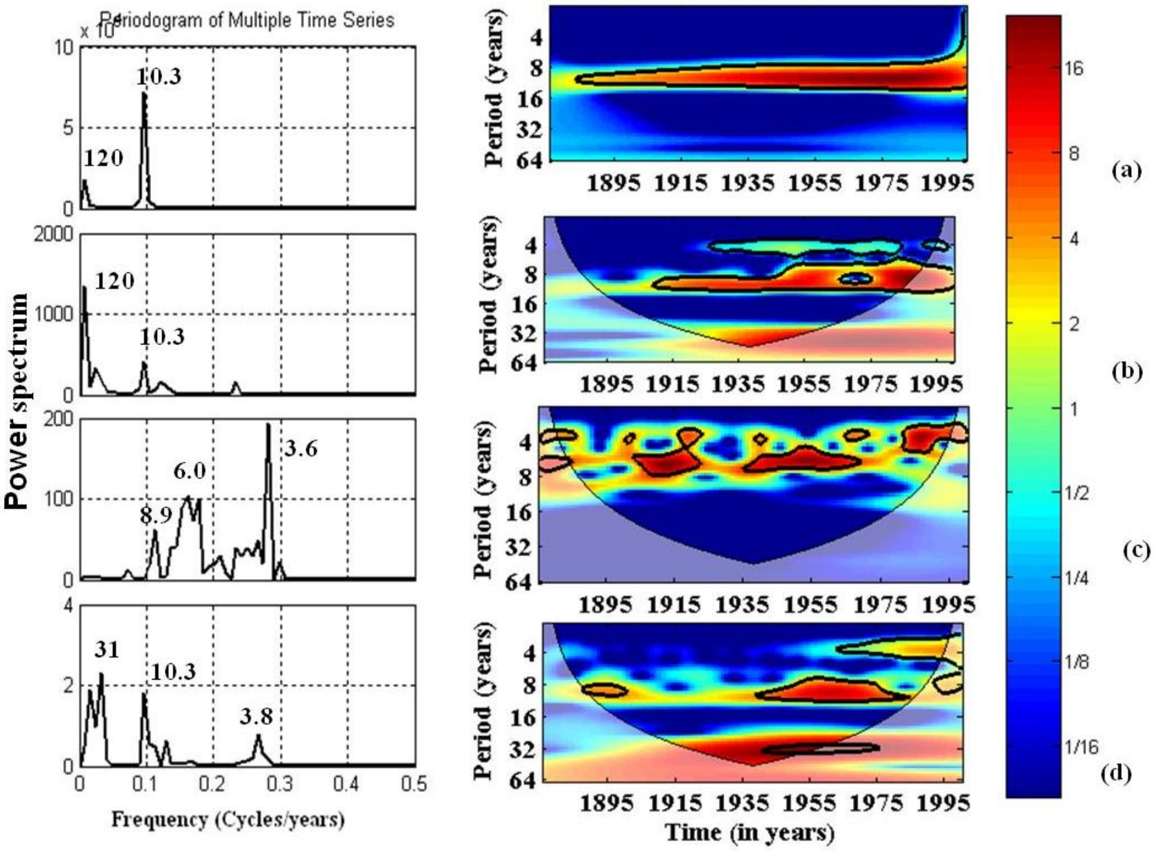

Figure 8. Power spectrum and Wavelet power spectrum of SSA reconstructed (a) Sunspot data (b) Geomagnetic Indices (aa index) (c) SOI index and (d) the Western Himalayas temperature data with cone of influence (lighter shade smooth curve) and black lines indicate significant power on 95% level compared to red noise based on AR(1) coefficient. The legend on right indicates the cross-wavelet power.

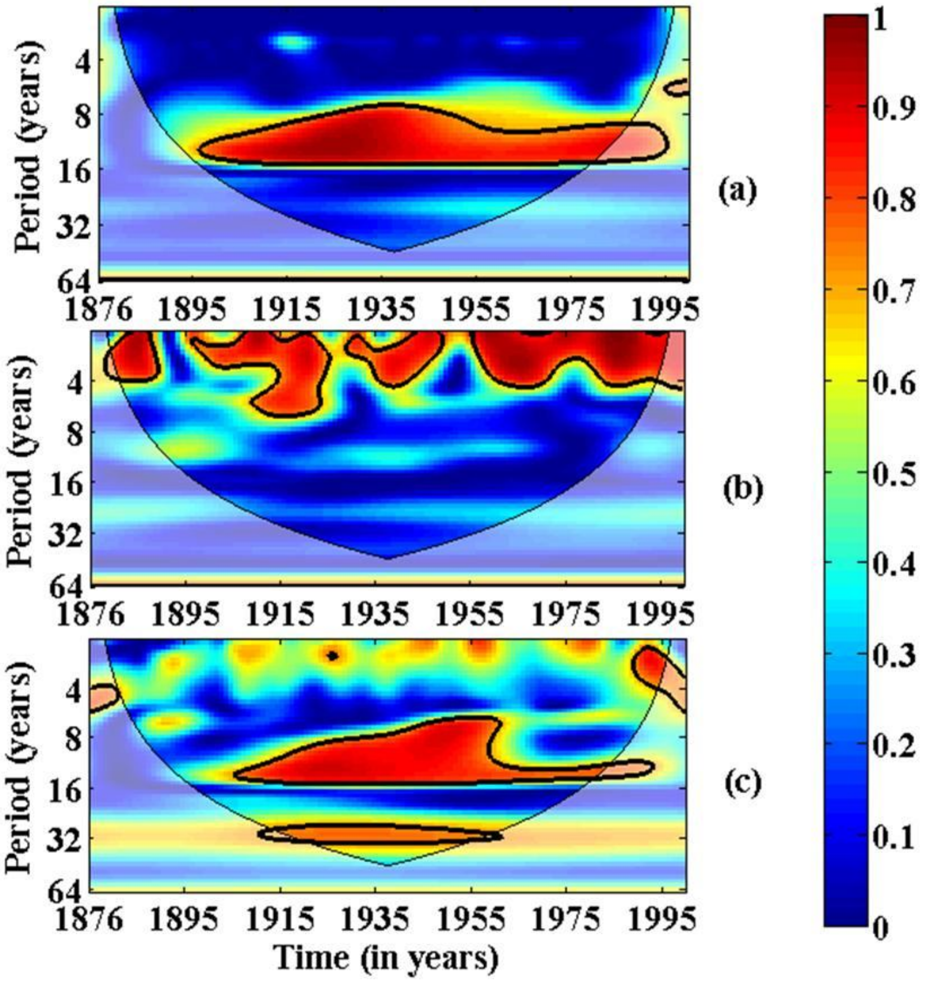

Figure 9. Squared wavelet coherence plotted for the SSA reconstructed time series between (a) WH-SSN (b) WH-SOI and (c) WH-aa index with cone of influence (lighter shade smooth curve) and black lines indicate significant power on 95% level compared to red noise based on AR(1) coefficient.

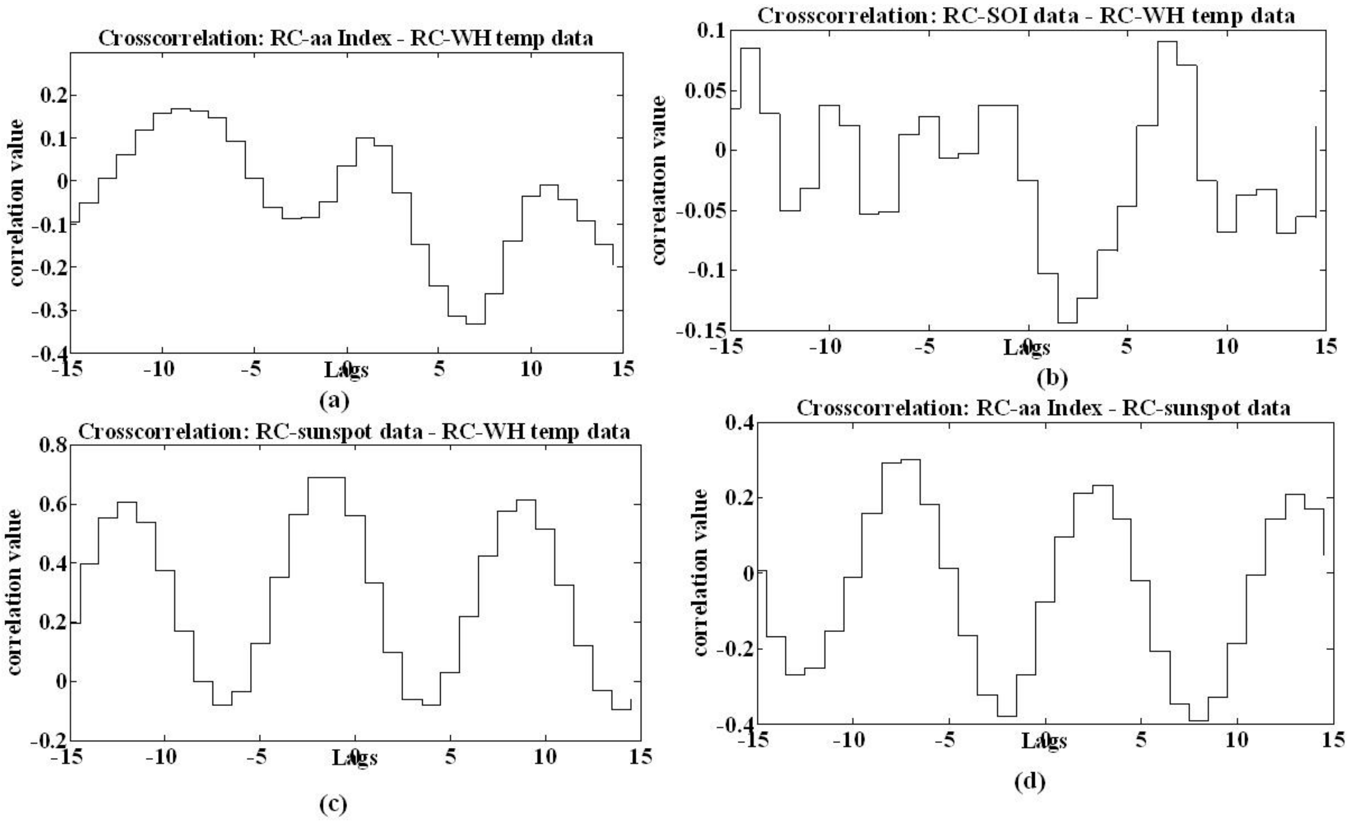

Figure 10. Cross-correlation of SSA reconstructed time series of (a) aa Index-Western Himalayan (WH) temperature data; (b) SOI-WH temperature data; (c) sunspot –WH data and (d) aa Index-sunspot data.